Journal of Materials Chemistry A

Accepted Manuscript

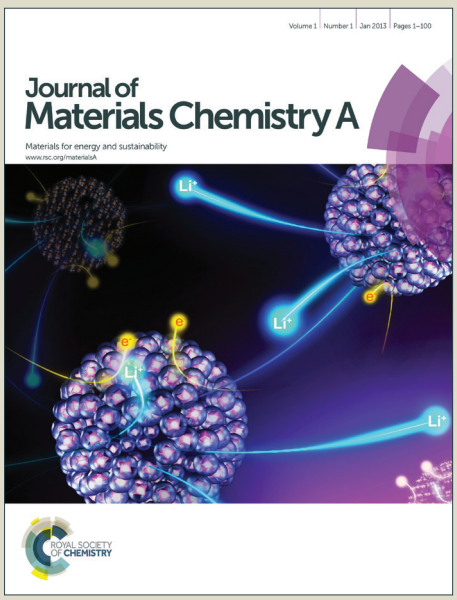

ROYAL SOCIETY OF CHEMISTRY

www.rsc.org/materialsA

Journal of Materials Chemistry A RSCPublishing

ARTICLE

Microwave-Assisted preparation of self-doped TiO_2 nanotube arrays for enhanced photoelectrochemical water splitting

Cite this: DOI: 10.1039/x0xx00000x

Received 00th January 2014,
Accepted 00th January 2014

DOI: 10.1039/x0xx00000x

www.rsc.org/

Hui Li, Jiangqiong Chen, Zhengbin Xia*, Junheng Xing

We report a microwave-assisted chemical reduction method with $NaBH_4$ to prepare bulk abundant Ti^{3+} self-doped TiO_2 nanotube arrays (MR-TNTs). UV-vis diffuse reflection spectra show the light absorption spectrum range of MR-TNTs extends from UV to visible light region and the electrochemical impedance spectra indicating the induced oxygen vacancies of MR-TNTs enhance their electrical conductivity as well as well as charge transfer. The MR-TNTs show 8-fold increase in visible light photocurrent density compared to the pristine TNTs, and the optimized saturation photocurrent density and photoconversion efficiency under AM 1.5 irradiation is identified to be 3.05 mA/cm^2 at 1.23 V vs. RHE and 1.66% respectively, which are the highest values ever reported for doped TNTs photoelectrodes. The incident photon to current conversion efficiency (IPCE) spectrum increase both in UV and visible light region. Moreover, the MR-TNTs exhibit much more stable PEC performance than the $NaBH_4$ treated TNTs without microwave assistance, which is attributed to the self-doped Ti^{3+} mainly exist in the bulk rather than on the surface.

Introduction

Solar-driven photoelectrochemical (PEC) water splitting by using semiconductor photocatalysts is one of the most promising approaches for clean hydrogen production.[1] Among all of semiconductors, TiO_2 has been extensively studied as photoelectrodes in the PEC system due to its appropriate band edge position, high chemical and thermal stability, and low cost.[2] However, the water splitting efficiency of TiO_2 based photoanodes is still unsatisfactory due to its limited light absorption spectrum range and fast photogenerated electron-hole pairs recombination.[3] To address these limitations, doping pristine TiO_2 with various impurity species (such as N, P, and F) by treating samples in according atmosphere or solutions has been demonstrated to be a feasible strategy to improve its PEC activity.[4-6] Unfortunately, the doped impurity species in TiO_2 often lead to severe thermal instability and relatively fast carriers recombination rate since the foreign introduced atoms can serve as carriers recombination centers, which undoubtedly impair the overall water splitting photoconversion efficiency of TiO_2 photoelectrodes.[7,8] Recently, the Ti^{3+} self-doped TiO_2 has attracted much interest due to it not only enhances visible light absorption because of the interband level of the Ti^{3+} (oxygen vacancy) but also increases electrical conductivity owing to high donor density, thus leading to significantly enhanced PEC water splitting performance under UV, visible light, and/or whole solar spectrum compared with pure samples.[9,10]

The previously reported methods to prepare self-doped TiO_2 are mainly focus on high-temperature heating in reducing gas (such as H_2[9,10], CO[11]) or melted aluminium,[12] hydrothermal synthesis,[13-15] flame[16] or plasma treatments,[17,18] and high energy bombardment (such as e-beam[19]). Although these methods have their own merits, they are severely limited by high cost and complicated procedures and not suitable for practical application. Moreover, for the promising one dimensional TiO_2 nanostructures (such as nanowires, nanotubes and nanobelts), above harsh treatments are not appropriate for them since their one dimensional morphologies and structures are easily destroyed. Thus, a facial, mild, and scalable method to produce stable self-doped TiO_2 photocatalysts is still much needed.

Very recently, Ye et al.[20] reported a facial one-step chemical method to synthesize partially reduced TiO_2 nanotube arrays. The mild chemical reduction with $NaBH_4$ under room temperature and pressure introduces oxygen

vacancies on the surface and interior of TiO_2, thus significantly enhancing the PEC water splitting performance of TiO_2 nanotube arrays photoelectrodes. However the Ti^{3+} doping concentration is still much low thus only creates localized oxygen vacancy states that usually deteriorate the electron mobility and exhibit negligible visible light photoactivity. In addition, most of the self-doped Ti^{3+} exist on the surface rather than in the bulk of TiO_2, which leading to moderate PEC enhancement and unstability due to that the surface Ti^{3+} easily oxidized by air or dissolved oxygen in water. Therefore, it is highly demanded to increase both the overall and bulk Ti^{3+} doping concentration of TiO_2 based on the $NaBH_4$ chemical reduction.

Herein, we develop a microwave-assisted chemical reduction method with $NaBH_4$ to prepare bulk abundant Ti^{3+} self-doped TiO_2 nanotube arrays (MR-TNTs). The highly ordered one dimensional TiO_2 nanotube arrays (TNTs) are rationally selected as pristine TiO_2 candidates because of their excellent PEC water splitting performance as well as their simple preparation.[21] The formation process of Ti^{3+} in the bulk is quickly achieved with microwave assistance owing to its fast and well-controlled heating rate, homogeneous heating distributing, and energy efficiency.[22,23] As a result, the MR-TNTs exhibit much higher PEC water splitting performance than the pristine TNTs and the $NaBH_4$ treated TNTs without microwave assistance (R-TNTs).

Experimental

Preparation of the self-doped MR-TNTs

Highly ordered MR-TNTs were firstly prepared by two-step anodization method[24,25] and then reduced by $NaBH_4$ aqueous solution with microwave assistance (scheme 1).

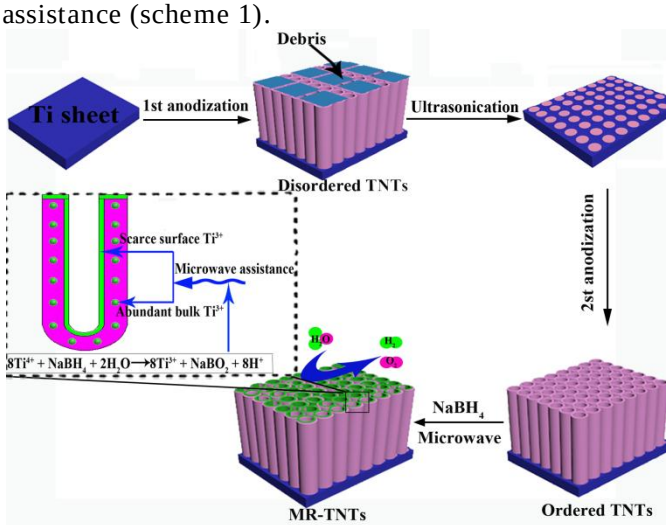

Scheme 1 Schematic diagram of the bulk abundant Ti^{3+} self-doped TNTs fabricated via two-step anodization method followed by microwave-assisted $NaBH_4$ treatment.

Briefly, a two-electrode electrochemical cell, with a working electrode of Ti foil and a counter electrode of Pt foil, was used for the preparation of TiO_2 nanotube arrays (TNTs). The titanium foils (purity 99.6%, thickness 1.0 mm) were firstly anodized in ethylene glycol (EG) electrolyte containing 0.5 wt% NH_4F and 2 vol% deionized water under 60 V for 2 h. Then the as-prepared TiO_2 layer was peeled off by ultrasonication in deionized water. Subsequently, the well-patterned titanium foils were subjected to a second anodization in the same electrolyte at 60 V for1 h. Finally, the as-anodized TNTs were annealed in air at 450 ^{o}C for 2 h. Finally, the annealed samples were dipped in 0.5 M $NaBH_4$ aqueous solution and heated with a microwave synthesizer for 10 min. The pristine TNTs and treated with $NaBH_4$ without microwave assistance (R-TNTs) were used to as references.

Characterization

The morphologies of the samples were characterized by field-emission scanning electron microscopy (FE-SEM) (NOVA NANOSEM 430, Holland) at an acceleration voltage of 15 kV. X-ray diffraction (XRD) patterns were obtained on an X-ray diffractometer (Bruker D8 ADVANCE, Germany) using Cu Kα radiation and operating at 40 kV/40 mA. The Raman spectra were recorded by a LabRAM Aramis (HORIBA Jobin Yvon, France) instrument, which was performed with the incidence power of 10.4 mW and the excitation wavelength of 532 nm. The UV-Vis light absorption spectra were obtained from a Hitachi UV-3010 spectrophotometer (Japan) equipped with an integrating sphere assembly and using $BaSO_4$ as a reference to measure all the samples. X-ray photoelectron spectrometry (XPS, Kratos Axis Ultra DLD, UK) was used to detect the surface chemical composition of the as-prepared samples. The spectral positions were corrected by normalizing the C 1s spectrum at 284.6 eV, and a Shirley background was used for the peak fitting. The Electron Paramagnetic Resonance (EPR) of the samples was recorded to confirm the bulk Ti^{3+} and oxygen vacancy on a JES-FA200 Electron Spin Resonance Spectrometer.

Photoelectrochemical activity measurement

PEC measurements were carried out in 1 M KOH electrolyte with a standard three-electrode cell of the obtained sample, platinum foil and Ag/AgCl as the working, counter and reference electrode, respectively. The potential and photocurrent of the photoelectrode were controlled by a potentiostat and were reported against the reversible hydrogen electrode (RHE):

$$E_{RHE} = E_{Ag/AgCl} + 0.059\ pH + E^{o}_{Ag/AgCl} \text{ with } E^{o}_{Ag/AgCl} = 0.1976\ V \text{ at } 25^{o}C \quad (1)$$

The samples were illuminated by a stimulated solar light (AM1.5, 100 mW/cm^2) or visible light (λ > 400 nm, 100 mW/cm^2) were provided by a PLS-SXE300UV Xe

lamp (Changtuo, China). The intensity of the light source was measured by a radiant power meter (Instruments of Beijing Normal University) and the visible light was obtained using a UV-400 optical filter. The photocurrent response under 1.23 V vs. RHE was recorded with an Agilent digital multimeter. The scan rate for the linear sweep voltammetry (LSV) was 5mV/s. The incident-photon-to-current-conversion efficiency (IPCE) measurements were performed without external bias in a two-electrode model, with prepared samples as anode, and Pt as cathode. The electrochemical spectra (EIS) were performed under illumination (100 mW/cm^2) at open circuit voltage over a frequency range from 10^5 to 0.1 Hz with an AC voltage at 10 mV. Simultaneously, the Mott-Schottky plots were obtained at a fixed frequency of 5 kHZ to determine the flat band potential and carrier density. All experiments were carried out under ambient conditions.

Results and discussion

The scanning electron microscopy (SEM) images of the pristine TNTs, MR-TNTs are shown in Fig. 1. The bare TNTs have a well-ordered, and uniform-arranged tubular structure with an average internal pore diameter of 125 nm and a length of about 14 μm (Fig. 1a, b). After $NaBH_4$ treatment with microwave assistance, Fig. 1c, d show the TNTs keep their top high-density porous morphology (tube diameter, wall thickness) and cross-sectional tubular structure (tube length, dimension), which indicates the mild reduction process has not changed the nanostructure of TNTs. The top-porous and bottom-tubular nanostructure is beneficial for broadband light confinement and unidirectional electron transport.

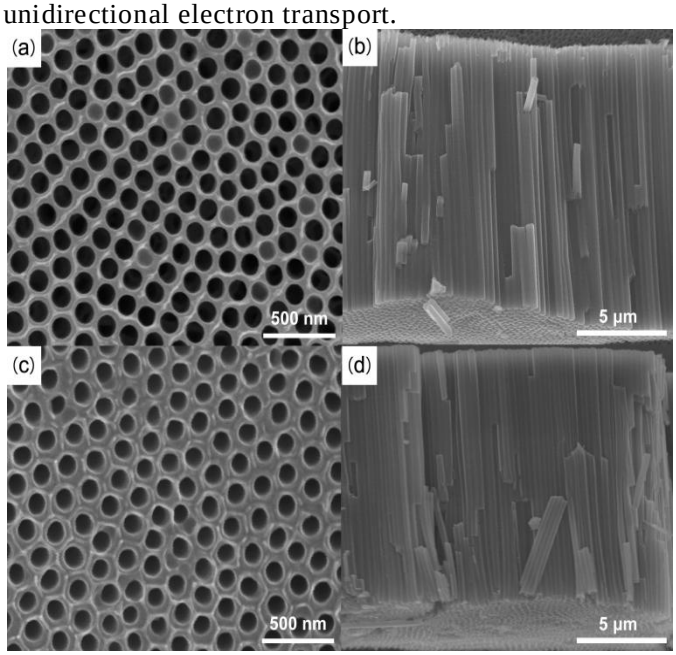

Fig. 1 Top (left row) and cross-sectional (right row) SEM images of (a, b) the pristine TNTs and MR-TNTs.

X-ray diffraction (XRD) was employed to the crystal phase of the pure TNTs and MR-TNTs. Clearly showing in Fig. 2, XRD diffraction peaks located at 25.3 °, 37.8 °, 47.9 °, 54.0 ° suggest that the annealed TNTs are highly crystallized with pure anatase phase.[26,27] After the microwave-assisted chemical reduction, the MR-TNTs also exhibit strong anatase diffraction, but a close observation of the XRD pattern in the range of 20 to 30 °, a broad peak centered at 20.8 ° and a sharp peak located at 27.2 ° (inset of Figure 2a). These peaks can be identified as the reduced TiO_2 species (such as Ti_4O_7), indicating that the TNTs actually have reacted with the $NaBH_4$ molecular and formed corresponding products.[28]

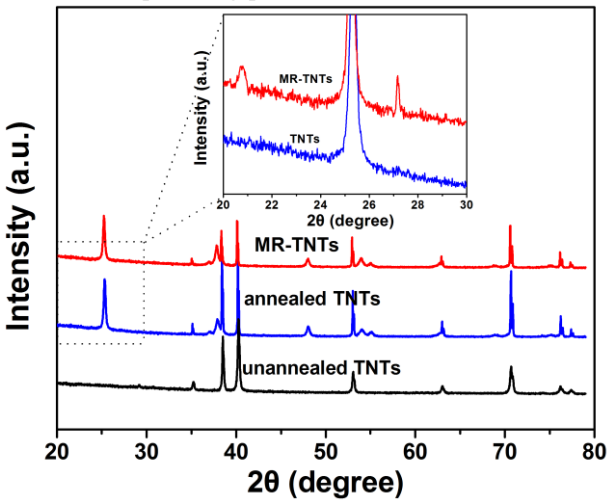

Fig. 2 XRD patterns of unannealed TNTs, annealed TNTs, and MR-TNTs, the inset is a magnification view in range of 20-30 °.

X-ray photoelectron spectroscopy (XPS) is a powerful tool to investigate the change of surface chemical bonding. As shown in Fig. 3a, the peak of O 1s XPS spectra exhibits a slight shift to lower energy (from 529.8 to 529.2 eV) after the chemical reduction, which may be the result of the electrons transfer from conduction band to oxygen vacancies state.[29] The Ti 2p XPS spectra are almost identical for the pure TNTs with Ti $2p_{3/2}$ and Ti $2p_{1/2}$ peaks located at binding energies of 458.6 and 464.3 eV, which are typical for the Ti^{4+}-O bonds in TiO_2 (Fig. 3b).[24] Clearly, no Ti^{3+} species are detected by XPS since the surface Ti^{3+} can be easily oxidized back to Ti^{4+} by oxygen in water or air and the XPS technique only probes the surface composition (1-10 nm) of a material.[30,31] Thus we conduct the low temperature electron paramagnetic resonance (EPR) to further confirm the presence of bulk Ti^{3+}. As shown in Fig. 3c, the reduced samples (R-TNTs and MR-TNTs) give rise to obvious EPR signal, while no signal is seen for the pure TNTs. For the R-TNTs, the EPR signal with g value of 2.020 corresponding to O^{2-} induced from the reduction of

absorbed O_2 by surface Ti^{3+}, which suggests that the $NaBH_4$ chemical treatment without microwave assistance only generates Ti^{3+} on the surface of TNTs.[32] The presence of strong EPR signal at g= 1.958 for the MR-TNTs indicates abundant Ti^{3+} spins in the bulk of material.[11] Moreover, the EPR signal with g value of 2.020 for the MR-TNTs is much weaker than that of R-TNTs, which confirms most of Ti^{3+} exist in the bulk rather than on the surface and bulk Ti^{3+} is much more stable than the surface Ti^{3+}. All the above results sufficiently indicate that the microwave play vital role in forming abundant bulk Ti^{3+} during the chemical reduction process.

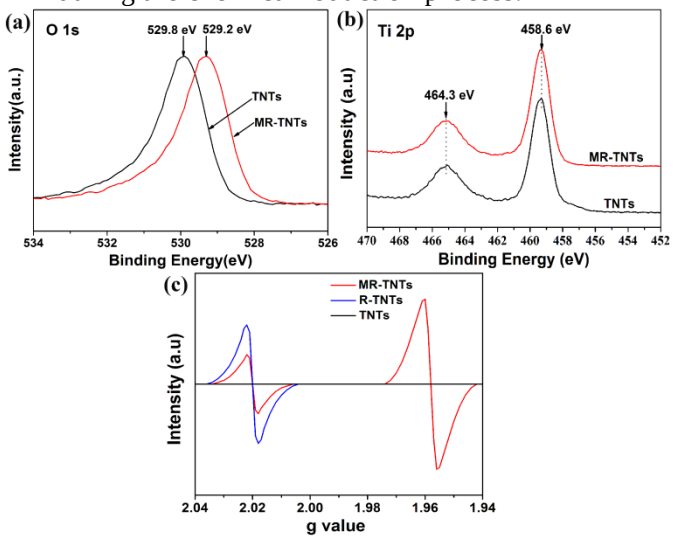

Fig. 3 (a) O 1s (b) Ti 2p XPS spectra of the pure TNTs and MR-TNTs. (c) EPR spectra of the pristine TNTs, R-TNTs, and MR-TNTs.

Transient photocurrent response measurements were performed over the pristine TNTs, R-TNTs, and MR-TNTs during repeated on/off visible light irradiation cycles at 1.23 V vs. RHE (Fig. 4a). Clearly, all the samples show fast and reproducible photocurrent response upon each cycle illumination. The transient photocurrent of the MR-TNTs is 0.242 mA/cm^2, which represents a 8-fold increase from the pristine TNTs (0.030 mA/cn^2). Simultaneously, the MR-TNTs show higher photocurrent density than that of R-TNTs (0.134 mA/cm^2). Moreover, the photocurrent response of the prepared samples under the simulated solar illumination (AM1.5, 100 mW/cm^2) show the same trend, is that the MR-TNTs exhibit much higher photocurrent value than the pristine TNTs and R-TNTs (Fig. S2). The linear sweep voltammetry (LSV) of the prepared samples was recorded under simulated solar light illumination (AM1.5, 100 mW/cm^2) and the results were shown in Fig. 4b. Upon illumination, the photocurrent density gradually increases with increasing applied potential from 0.1 to 0.9 V vs. RHE, suggesting photogenerated electron-hole pairs separation resulting from the electric field.[33] At higher potentials (E > 0.9 V), a saturation of the photocurrent is observed for all samples. In comparison with the pristine TNTs, the MR-TNTs exhibit about two times enhanced saturated photocurrent (3.05 mA/cm^2), which is the highest photocurrent density ever reported on doped TNTs photoelectrode under same situations. In addition, the onset potentials of R-TNTs and MR-TNTs shift negatively compared that of the pure TNTs, which may be due to that the materials possess the merits of lower band bending requirement for separating photogenerated electron-hole pairs and better charges transport.[34] The applied bias photoconversion efficiency of the prepared samples is calculated via the following equation[35]:

$$\varepsilon_0(\%) = j_p \frac{E^0_{rev} - |E_{app}|}{I_0} \times 100 \quad (2)$$

where ε_0 is the photoconversion efficiency, j_p is the photocurrent density (mA/cm^2), I_0 means the intensity of the incident light, E^0_{rev} represents the standard reversible potential (1.23 V vs. RHE), and $|E_{app}|$ denotes the absolute value of the applied voltage which is obtained from $E_{app} = E_{meas} - E_{aoc}$, where E_{meas} is the electrode potential (vs . Ag/AgCl) at which j_p is meas ured and E_{aoc} is the electrode potential (vs. Ag/AgCl) at open circuit under illumination. Plots of photoconversion efficiency with applied potential are shown in Fig. 4c. The maximum photoconversion efficiency of the TNTs is calculated to be 0.78 % at 0.82 V vs. RHE. Notably, the MR-TNTs achieve the highest efficiency of 1.66% at 0.78 V vs. RHE. Likewise, the R-TNTs exhibit the optimal efficiency of 0.85% at a similar applied bias. Based above results and discussion, we can conclude that the microwave-assisted $NaBH_4$ treatment significantly enhances photoconversion efficiency by improving the maximum photocurrent and shifts potential negatively.

To estimate the photoactivity of the prepared electrodes as a function of wavelength of incident light, the incident-photon-to-current-conversion efficiency (IPCE) measurements were performed with a two electrode system in the absence of external bias over the pristine TNTs, R-TNTs, and MR-TNTs. The IPCE values can be calculated by the following equation[36]:

$$\mathrm{IPCE} = (1240I)/\lambda J_{light} \quad (3)$$

where I, λ, and J_{light} are the photocurrent density, incident light wavelength, and measured irradiance, respectively. Fig. 4d shows that the reduced samples (MR-TNTs and TNTs) both exhibit significantly photoactivity in the UV region. Particularly, the MR-TNTs have the highest IPCE values of 92.8% at 350 nm, which is about 2.5 times higher than that of the pristine TNTs. It suggests that the UV light is effectively utilized for PEC water splitting.

Significantly, the MR-TNTs and R-TNTs all show significant photoactivity improvement within the visible light region (400-550 nm) compared to the pristine TNTs (inset of Fig. 4d), which can be attributed to narrowed band gap induced by Ti^{3+} (or oxygen vacancy) interband level between the valence band and conduction band of reduced TNTs. Moreover, the MR-TNTs show higher IPCE values over the entire light spectrum may be due to that the abundant bulk Ti^{3+} species are much more stable than the surface Ti^{3+} for efficiently facilitating the charge separation. The stability of the MR-TNTs and R-TNTs were investigated with amperometric *I-t* measurements under simulated solar light illumination with 60 s light on-off cycle. The photocurrent density of R-TNTs show obvious decay at the end of measurement, while that of MR-TNTs still keep stable state all the time (Fig. S1). The high stability of MR-TNTs can be mainly attributed to two reasons. The first reason is that the majority of Ti^{3+} species are significantly retained in the bulk of R-TNTs, which is reported to be more stable than those located on and near the surface. The second one is that the Ti^{3+} interband level locates just below the conduction band minimum of TiO_2, thus cannot be oxidized by the valence band holes.

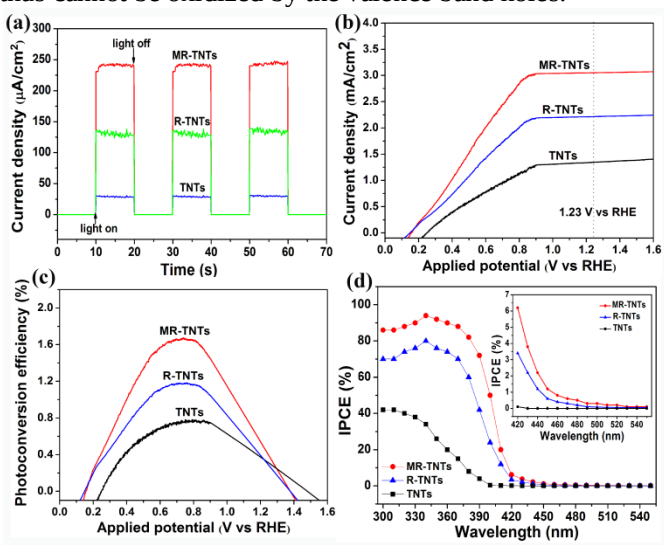

Fig. 4 Photoelectrochemical performance of the TNTs, R-TNTs, and MR-TNTs photoelectrodes: (a) amperometric *I-t* curves at an applied potential of 1.23 V (vs. RHE) under visible light illumination, (b) linear-sweep voltammograms with scanning rate of 5 mV/s, (c) photoconversion efficiency as a function of applied potentials under simulated solar light illumination (AM1.5, 100 mW/cm^2), and (d) IPCE spectra, collected at the incident wavelength range from 300 to 550 nm without external bias, inset is magnified IPCE spectra at the incident wavelength vary from 420 to 550 nm.

Electrochemical impedance spectra (EIS) were employed to investigate the charge separation and transport of the prepared samples. The EIS measurements were performed covering the frequency range of 10^5-0.1 Hz using an amplitude of 10 mV at the open circuit potential of the system. Fig. 5a presents typical Nyquist plots for the TNTs, R-TNTs, and MR-TNTs under illumination. It is clearly observed that the radius of the arc on the EIS Nyquist plots of MR-TNTs and R-TNTs are both lower than that of TNTs. This indicates that the reduced samples possess smaller charge transfer resistance and better photogenerated electron-hole pairs separation and mobility which may be ascribed to the presence of Ti^{3+} species on the surface or in the bulk of materials. Mott-Schottky (MS) plots were collected at 5 kHz in the dark to determine semiconductor type, flat band potential (E_{FB}) and carriers density (N_D) of the obtained samples following the equation below[37,38]:

$$\frac{1}{C^2} = \frac{2}{N_D e \varepsilon_0 \varepsilon}\left(E - E_{FB} - \frac{kT}{e}\right) \quad (4)$$

where C is the space charge capacitance in the semiconductor, N_D is the electron carriers density, e is the elemental charge, ε_0 is the permittivity of a vacuum, ε is the relative permittivity of the semiconductor, E is the applied potential, E_{FB} is the flat band potential, T is the temperature, and k is the Boltzmann constant. Fig. 5b displays the Mott-Schottky plots of $1/C^2$ as a function of the applied potential, from which the positive slopes of the linear parts of the curves are observed, suggesting n-type semiconductors. Furthermore, the plots are extrapolated to $1/C^2=0$ to estimate the values of E_{FB} for the TNTs, R-TNTs, and MR-TNTs are 0.28, 0.42, and 0.51 V, respectively. It is worth noting that the positive shift of E_{FB} in reduced TNTs implies a decrease in bending of the band edge, thus facilitating the photogenerated electron separation and transfer, which is accordance with many previous reports.[21,39,40] While in the previous literature,[20] the E_{FB} of $NaBH_4$ reduced sample shows a negative shift, which may be attributed to the minor different experimental test condition, that is, the Mott-Schottky of previous report may be conducted under the light illumination while the present study is performed at the dark condition. With the light participation, more charge are accumulating at the interface between semiconductor and electrolyte, which may eases the band bending in a certain degree and cause the negative shift of E_{FB}. The carrier density N_D was calculated from Fig. 5b using the following equation[24]:

$$N_D = \frac{2}{e\varepsilon_0\varepsilon}\left(\frac{dE}{d\left(\frac{1}{C^2}\right)}\right) \quad (5)$$

as e = 1.6×10^{-19} C, ε_0 = 8.86×10^{-12} F/m, and ε = 48 for anatase TiO_2,[41] the N_D values of TNTs, R-TNTs, and MR-TNTs are determined to be 2.16×10^{18}, 3.31×10^{18}, 5.59×10^{18} cm^{-3}, respectively. This indicates that the donor density of reduced TNTs is significantly increased because of the existence of Ti^{3+} that serves

as electron donors and the Ti^{3+} concentration of MR-TNTs is higher than that of R-TNTs. In a word, the electrical properties confirms that the bulk abundant Ti^{3+} self-doped MR-TNTs have better electrical conductivity than the TNTs and R-TNTs, which facilitates the charge separation and transfer and leads to PEC water splitting enhancement.

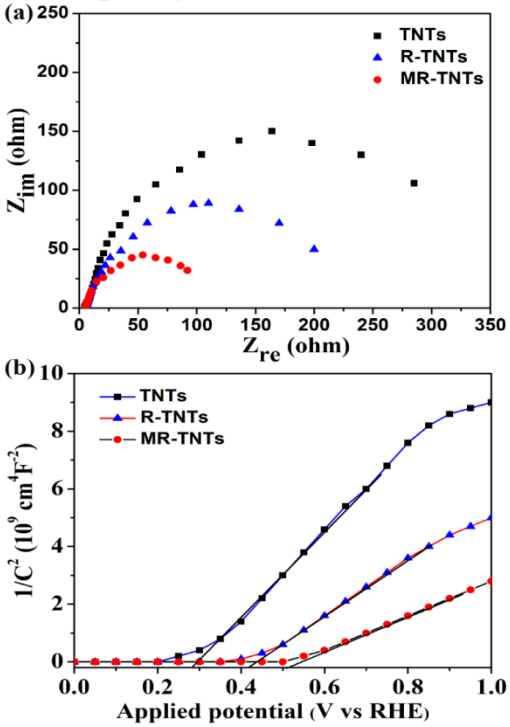

Fig. 5 (a) Electrochemical impedance spectra of Nyquist plots collected at open circuit potential under illumination, and (b) Mott-Schottky plots of the pristine TNTs, R-TNTs, and MR-TNTs at a frequency of 5 Hz in the dark.

Fig. 6a shows the UV-vis absorption spectra of the pristine TNTs, R-TNTs and MR-TNTs. The strong UV absorption of all samples is ascribed to the electronic transition from the valence band to the conduction band. The MR-TNTs and R-TNTs exhibit higher light absorbance than the pure TNTs in the visible light region and show a red shift in the absorption edges, which can be attributed to the electronic transition from the valence band to the Ti^{3+} induced interband or from this band level to the conduction band in the MR-TNTs. The band gap energy of pristine TNTs, R-TNTs and MR-TNTs estimated with the Kubelka-Munk function is about 3.10, 2.88 and 2.39 eV, respectively (Fig. 6a, inset). This band-gap narrowing for the MR-TNTs and R-TNTs is consistent with the assumption that an electronic band level is located just below the conduction band of reduced samples. Simultaneously, the bandgap of MR-TNTs is smaller than that of R-TNTs, which can be ascribed to that the self-doping Ti^{3+} of MR-TNTs mainly distributed in the bulk phase while that of R-TNTs centered in the surface region. This result definitely demonstrates the microwave assistance is a effective auxiliary mean to prepare the efficient self-doped photocatalysts. In addition, the bandgap of the present R-TNTs is large than that of its counterpart in the previous report[20] under the similar $NaBH_4$ reduction condition, which can be attributed to the different $NaBH_4$ concentration, that is, the current $NaBH_4$ concentration (0.5 M) is much higher than that of previous study (0.1 M). High concentration of $NaBH_4$ means high reduction ability and results in more reduced Ti^{3+} doped into the sample. The density of states (DOS) of the valence band (VB) of TNTs and MR-TNTs were also measured by valence band (VB) (Fig. 6b). The pure TNTs show the characteristic VB DOS of TiO_2, with the band edge of at about 2.05 eV below the Fermi energy. Since the optical band gap of the pristine TNTs is 3.10 (Fig. 6a, inset). The conduction band (CB) minimum would occur at -1.05 eV. On the other hand, the VB maximum of the MR-TNTs show shift to 1.75 eV and is followed by a tail toward about 1.32 eV. Considering the optical band gap of the MR-TNTs is 2.39 eV, thus its CB minimum would occur at -0.46 eV. A schematic illustration of the DOS of TNTs and MR-TNTs is vividly shown in Fig. 6c. The microwave-assisted chemical reduction introduces abundant oxygen vacancy into the bulk of MR-TNTs, which induces narrowed band gap and slight VB tailing. In addition, self-doped Ti^{3+} species introduce localized states below the CB minimum of MR-TNTs. Both the VB tailing and Ti^{3+} localized states of MR-TNTs are responsible for their significant visible light absorption.

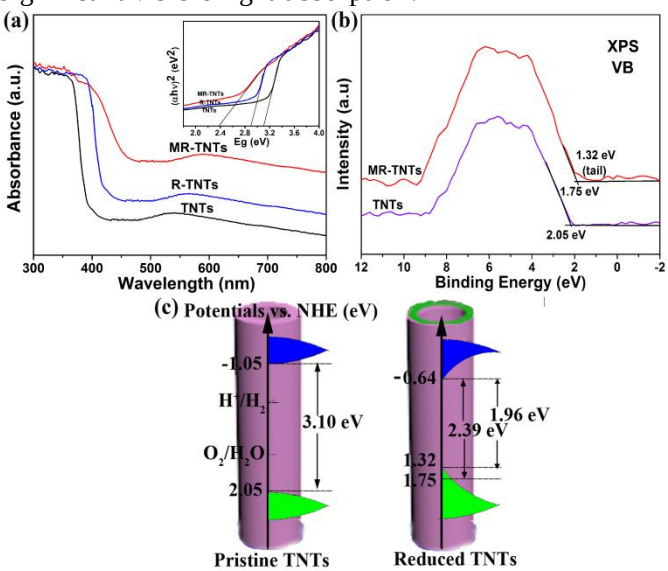

Fig. 6 (a) UV-vis diffuse reflection spectra, (b) valence-band XPS spectra, and (c) schematic illustration of the density of state of the pure TNTs and MR-TNTs. Inset in (a) is $(\alpha h\nu)^{0.5}$ vs. hν plots.

Conclusions

In all, our study demonstrates that the microwave-assisted $NaBH_4$ treatment is an effective and mild strategy to introduce abundant Ti^{3+} species into the bulk of TNTs and the MR-TNTs photoelectrodes show excellent and stable PEC water splitting performance as results of the efficient visible light absorption and fast charge separation. The optimized saturation photocurrent density and photoconversion efficiency of the MR-TNTs under simulated solar illumination are measured to be 3.05 mA/cm^2 and 1.66%, respectively, which are the highest values ever reported for doped TNTs photoelectrodes. The present work sheds light on the application of mild chemical reduction strategy to performance improvement for metal oxide based semiconductor in the fields of dye-sensitized soalr cells, PEC water splitting devices and supercapacitors.

Acknowledgements

This work was supported by the National Natural Science Foundation of China (NSFC, NO. 20976058).

Notes and references

School of Chemistry and Chemical Engineering, South China University of Technology, Guangzhou, Guangdong 510641, China

*E-mail address: cezhbxia@scut.edu.cn

Electronic Supplementary Information (ESI) available: Photocurrent density response stability of the prepared samples (Fig. S1). See DOI: 10.1039/b000000x/

1. X. Chen, S. Shen, L. Guo and S. S. Mao, *Chem. Rev.*, 2010, **110**, 6503.
2. J. Du, X. Lai, N. Yang, J. Zhai, D. Kisailus, F. Su, D. Wang and L. Jiang, *ACS Nano*, 2010, **5**, 590.
3. M. Nowotny, T. Bak and J. Nowotny, *J. Phys.Chem. B*, 2006, **110**, 16270.
4. R. Asahi, T. Morikawa, T. Ohwaki, K. Aoki and Y. Taga, *Science*, 2001, **293**, 269.
5. K. Yang, Y. Dai and B. Huang, *J. Phys.Chem. C*, 2007, **111**, 18985.
6. A. Czoska, S. Livraghi, M. Chiesa, E. Giamello, S. Agnoli, G. Granozzi, E. Finazzi, C. D. Valentin and G. Pacchioni, *J. Phys.Chem. C*, 2008, **112**, 8951.
7. O. Diwald, T. L. Thompson, T. Zubkov, E. G. Goralski, S. D. Walck and J. T. Yates, *J. Phys.Chem. B*, 2004, **108**, 6004.
8. A. Naldoni, M. Allieta, S. Santangelo, M. Marelli, F. Fabbri, S. Cappelli, C. L. Bianchi, R. Psaro and V. Dal Santo, *J. Am. Chem. Soc.*, 2012, **134**, 7600.
9. X. Chen, L. Liu, Y. Y. Peter and S. S. Mao, *Science*, 2011, **331**, 746.
10. G. Wang, H. Wang, Y. Ling, Y. Tang, X. Yang, R. C. Fitzmorris, C. Wang, J. Z. Zhang and Y. Li, *Nano Lett.*, 2011, **11**, 3026.
11. F. Zuo, L. Wang, T. Wu, Z. Zhang, D. Borchardt and P. Feng, *J. Am. Chem. Soc.*, 2010, **132**, 11856.
12. H. Cui, W. Zhao, C. Yang, H. Yin, T. Lin, Y. Shan, Y. Xie, H. Gu and F. Huang, *J. Mater. Chem. A*, 2014, **2**, 8612.
13. F. N. Sayed, O. Jayakumar, R. Sasikala, R. Kadam, S. R. Bharadwaj, L. Kienle, U. Schürmann, S. r. Kaps, R. Adelung and J. Mittal, *J. Phys.Chem. C*, 2012, **116**, 12462.
14. X. Liu, S. Gao, H. Xu, Z. Lou, W. Wang, B. Huang and Y. Dai, *Nanoscale*, 2013, **5**, 1870.
15. Q. Zhu, Y. Peng, L. Lin, C.-M. Fan, G.-Q. Gao, R.-X. Wang and A.-W. Xu, *J. Mater. Chem. A*, 2014, **2**, 4429.
16. I. S. Cho, M. Logar, C. H. Lee, L. Cai, F. B. Prinz and X. Zheng, *Nano Lett.*, 2013, **14**, 24.
17. Z. Wang, C. Yang, T. Lin, H. Yin, P. Chen, D. Wan, F. Xu, F. Huang, J. Lin and X. Xie, *Adv. Funct. Mater.*, 2013, **23**, 5444.
18. F. Teng, M. Li, C. Gao, G. Zhang, P. Zhang, Y. Wang, L. Chen and E. Xie, *Appl. Catal. B: Environ.*, 2014, **148–149**, 339.
19. M. Mansoob, S. A. Ansari, D. Pradhan, D. Han, J. Lee and M. Cho, *J. Mater. Chem. A*, 2014, **2**, 637.
20. Q. Kang, J. Cao, Y. Zhang, L. Liu, H. Xu and J. Ye, *J. Mater. Chem. A*, 2013, **1**, 5766.
21. Z. Zhang and P. Wang, *Energ. Environ. Sci.*, 2012, **5**, 6506.
22. R. C. Coffin, J. Peet, J. Rogers and G. C. Bazan, *Nat. Chem.*, 2009, **1**, 657.
23. L. Pan, X. Liu, Z. Sun and C. Q. Sun, *J. Mater. Chem. A*, 2013, **1**, 8299.
24. H. Li, J. Xing, Z. Xia and J. Chen, *Electrochim. Acta*, 2014, **139**, 331.
25. H. Li, J. Xing, Z. Xia and J. Chen, *RSC Adv.*, 2014, **4**, 23214.
26. J. Xing, H. Li, Z. Xia, J. Chen, Y. Zhang and L. Zhong, *Ind. Eng. Chem. Res.*, 2014, **53**, 10667.
27. J. Xing, H. Li, Z. Xia, J. Chen, Y. Zhang and L. Zhong, *Electrochim. Acta*, 2014, **134**, 242.
28. A. Kitada, G. Hasegawa, Y. Kobayashi, K. Kanamori, K.Nakanishi and H. Kageyama, *J. Am. Chem. Soc.*, 2012, **134**, 10894.
29. M. A. Henderson, W. S. Epling, C. H. F. Peden and C. L. Perkins, *J. Phys.Chem. B*, 2002, **107**, 534.
30. A. Teleki and S. E. Pratsinis, *Phys. Chem. Chem. Phys.*, 2009, **11**, 3742.
31. F. Zuo, K. Bozhilov, R. J. Dillon, L. Wang, P. Smith, X. Zhao, C. Bardeen and P. Feng, *Angew. Chem. Int. Ed.*, 2012, **51**, 6223.
32. S. M. Prokes, J. L. Gole, X. Chen, C. Burda and W. E. Carlos, *Adv. Funct. Mater.*, 2005, **15**, 161.
33. N. K. Allam, K. Shankar and C. A. Grimes, *J. Mater. Chem.*, 2008, **18**, 2341.
34. S. Hoang, S. Guo, N. T. Hahn, A. J. Bard and C. B. Mullins, *Nano Lett.*, 2011, **12**, 26.
35. S. U. M. Khan, M. Al-Shahry and W. B. Ingler, *Science*, 2002, **297**, 2243.
36. T. Bak, J. Nowotny, M. Rekas and C. C. Sorrell, *Int. J. Hydrogen Energy*, 2002, 27, 991.
37. G. Wang, Q. Wang, W. Lu and J. Li, *J. Phys.Chem. B*, 2006, **110**, 22029.
38. R. O'Hayre, M. Nanu, J. Schoonman and A. Goossens, *J. Phys.Chem. C*, 2007, **111**, 4809.
39. Z. Zhang, M. N. Hedhili, H. Zhu and P. Wang, *Phys. Chem. Chem. Phys.*, 2013, **15**, 15637.
40. N. Zhang, Y. Zhang, X. Pan, M. Q. Yang and Y. J. Xu, *J. Phys. Chem. C*, 2012, **116**, 18023.
41. P. K. Ghosh and M. E. Azimi, Dielectrics and Electrical Insulation, *IEEE Transactions on*, 1994, **1**, 975.

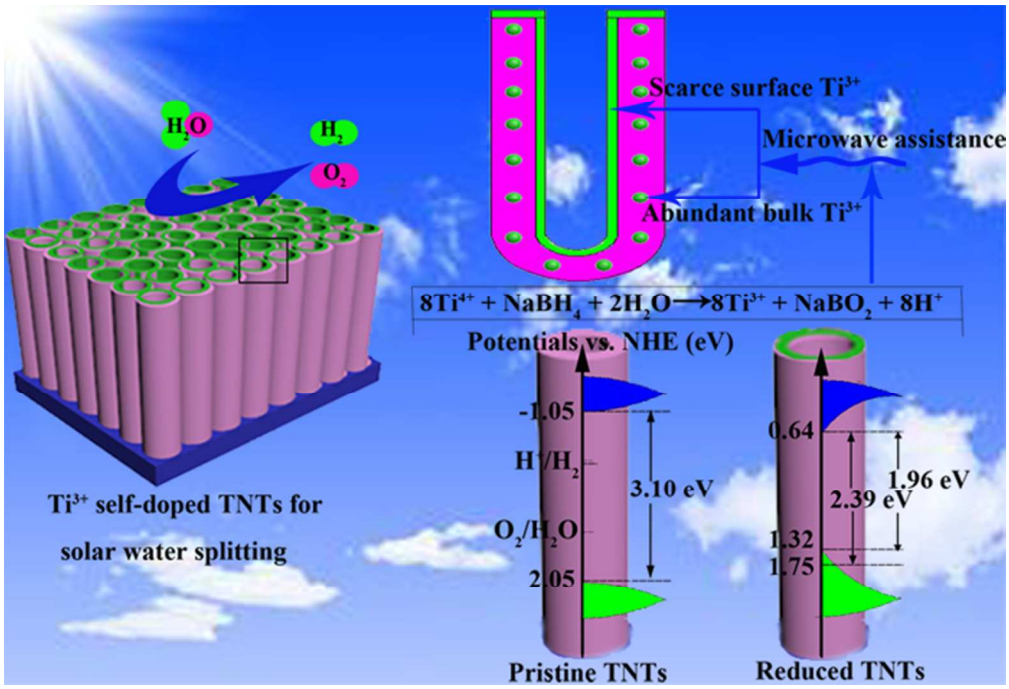

Bulk abundant Ti3+ self-doped TiO2 nanotube arrays are prepared by a microwave-assisted chemical reduction method with NaBH4
58x39mm (300 x 300 DPI)